A spatio-temporal model for temporal evolution of spatial extremal dependence

Véronique Maume-Deschamps, Pierre Ribereau, Manal Zeidan

A spatio-temporal model for temporal evolution of spatial extremal dependence

Véronique MAUME-DESCHAMPS[a], Pierre RIBEREAU[a], Manal ZEIDAN[a,b,*]

[a] *Universite Claude Bernard Lyon 1, CNRS, Ecole Centrale de Lyon, INSA Lyon, Université Jean Monnet, ICJ, UMR5208, Villeurbanne, 69622, France*
[b] *Department of Operation Research and Intelligent techniques, University of Mosul, Mosul, 41002, Iraq*

Abstract

Few spatio-temporal models allow temporal non-stationarity. When modeling environmental data recorded over the last decades of the 20th century until now, it seems not reasonable to assume temporal stationarity, since it would not capture climate change effects. In this paper, we propose a space-time max-stable model for modeling some temporal non-stationarity of the spatial extremal dependence. Our model consists of a mixture of max-stable spatial processes, with a rate of mixing depending on time. We use maximum composite likelihood for estimation, model selection, and a non-stationarity test. The assessment of its performance is done through wide simulation experiments. The proposed model is used to investigate how the rainfall in the south of France evolves with time. The results demonstrate that the spatial extremal dependence is significantly non-stationary over time, with a decrease in the strength of dependence.

Keywords: Spatio-temporal processes, Max-stable mixture processes, Non-stationary extremal dependence, Climate change.

*Corresponding author
Email addresses: veronique.maume@univ-lyon1.fr (Véronique MAUME-DESCHAMPS), pierre.ribereau@univ-lyon1.fr (Pierre RIBEREAU), manal.zeidan@univ-lyon1.fr (Manal ZEIDAN)

1. Introduction

In recent years, climate change has significantly impacted the nature of environmental extreme events. This requires the construction of statistical models, able to represent time-varying extreme events. In this paper, we focus on studying the temporal non-stationarity of the spatial extremal dependence. Indeed, assuming it is stationary when modeling environmental extreme events, recorded over a long time is questionable. We consider max-stable processes which provide suitable models for representing extremal dependence structures for spatial extremes (De Haan, 1984; De Haan and Ferreira, 2006). Different spatial max-stable models were presented in the literature (Smith, 1990; Schlather, 2002; Kabluchko et al., 2009; Opitz, 2013), and in all of them, the extremal dependence was assumed to be temporal stationary. These models have been applied to various variables, e.g. rainfall, snow, and so on, see for example Padoan et al. (2010); Blanchet and Davison (2011); Gaume et al. (2013); Fawcett and Walshaw (2014); Saunders et al. (2017). Few papers deal with space-time max-stable models, see e.g. Davis et al. (2013); Huser and Davison (2014); Embrechts et al. (2016); Buhl and Klüppelberg (2016); Abu-Awwad et al. (2021), in which a stationary spatio-temporal dependence structure is assumed, considering a short-range temporal dependence.

The first paper which addresses the issue of the temporal non-stationarity of the spatial dependence structure was presented by Nicolet et al. (2016). The authors studied the impact of climate change on the dependence structure of extreme snowfall in the French Alps. They used an approach based on the data, called moving time windows, to estimate the extremal dependence. For each window, the range and smooth parameters of the Brown-Resnick model were estimated by fitting its theoretical extremal function using the least square method. The results detected a significant trend in spatial extremal dependence, where the snowfall extremes become less spatially dependent with time. Although this approach was able to detect the temporal trend in the spatial extremal dependence, it did not allow modeling of that trend. Afterward, Blanchet et al. (2018) studied the spatial dependence of extreme rainfall over West Africa. They investigated the temporal evaluation of the spatial extremal dependence using the moving time windows approach rather than modeling its trend. They fitted a stationary Brown-Resnick model for each time window using the pairwise maximum likelihood estimator. In Nicolet et al. (2018), a Brown-Resnick max-stable model with a temporal linear

trend in the range and smooth parameters of the spatial extremal dependence is proposed. It allows to consider some covariates to model the trends. The authors applied it on the extreme snow depth data of the French Alps, to assess the effect of climate change on its spatial dependence. They concluded that extremal dependence has a strong negative trend over time.

In this paper, we propose a novel space-time max-stable model for modeling the temporal nonstationarity in spatial extremal dependence. The idea behind constructing this model came from the notion that one possible way to create a non-stationary model is to form a mixture of max-stable models (Huser and Genton, 2016). This approach may provide a more realistic and accurate representation of extreme events. Our model represents a mixture of two spatial max-stable processes, with mixing proportion varying across time. It is a flexible model, as it can combine any two max-stable models, with time-varying mixing proportion modeled using any function (linear or non-linear) to construct the best space-time model representing the data. Throughout this paper, we assumed that the time-varying mixing proportion was modeled by a function representing a linear trend. For statistical inference, the maximum composite likelihood estimator (MCLE) was used to estimate the parameters of the proposed model. We assess its performance through several simulation experiments.

Moreover, statistic hypothesis tests are essential tools in statistics for model validation, in particular for complex models like max-stable models. Abu-Awwad et al. (2020) proposed two test statistics for the value of the mixing proportion parameter of a max-mixture model. Following this path, we propose a test statistic on the values of time-varying mixing proportion parameters of our proposed model, intending to validate the existence of a temporal trend. We performed extensive simulations to calculate the empirical power of our proposed test statistic.

Afterward, we use the proposed space-time max-stable model to study the time variation on the extreme rainfall in the south of France, where the majority of extreme rainfall occurs in this area as a result of this area being affected by the disturbances of the Mediterranean Sea and the Atlantic Ocean. This area was studied also by Oesting and Naveau (2020).

The rest of the paper is organized as follows. In Section 2 we present our proposed space-time max-stable model, with its two measures of extremal dependence: time-varying extremal function and time-varying F-madogram. Section 3 reviews the maximum composite likelihood estimator (MCLE) for statistical inference and its associated model selection criterion. In Section 4

we present several simulation experiments to evaluate the performance of the estimator and the test statistic. We detail the application of our proposed model to study the extreme rainfall over the south of France in Section 5. Lastly, the discussion and conclusion are enclosed in Section 6.

2. Time-varying max-stable mixture model

Let us begin with a short review on principles and definitions of max-stable processes, which are the base for the construction of the proposed model.
Let $\{Z_i(s), s \in \mathcal{S} \subset \mathbb{R}^d\}$, $d \geq 1$ and $i = 1, 2, \cdots$ be independent and identical distributed replicates of a spatial process $Z(s)$, assume there exist continuous functions $A_n(s) > 0$ and $B_n(s) \in \mathbb{R}$, so that

$$\bigvee_{i=1}^{n} \frac{Z_i(s) - B_n(s)}{A_n(s)} \xrightarrow{\mathcal{D}} X(s), s \in \mathcal{S}, n \to \infty, \tag{1}$$

where $\bigvee$ represents the max-operator. The limiting process $X(s)$ is assumed to have non-degenerate marginals, such a process is called a max-stable process (De Haan and Pereira, 2006). The univariate marginal distribution of $X(s)$ is a generalized extreme value distribution, i.e $X(s) \sim GEV(\mu(s), \sigma(s), \xi(s))$ with distribution function defined for all $x \in \mathbb{R}$ as:

$$\mathbb{P}(X(s) \leq x) = \exp[-(1 + \xi(s)\frac{x - \mu(s)}{\sigma(s)})^{-1/\xi(s)}], \;\; \sigma(s) > 0, \, \mu(s), \xi(s) \in \mathbb{R} \tag{2}$$

where $\mu(s)$, $\sigma(s)$, and $\xi(s)$ are the location, scale, and shape parameters, respectively for location s. When the marginal distributions of the process $\{X(s), s \in \mathcal{S}\}$ are unit Fréchet distributions with distribution function $\mathbb{P}(X(s) \leq x) = \exp[-1/x], x > 0$ (corresponding to $X(s) \sim GEV(1, 1, 1)$ for all $s \in \mathcal{S}$), the process is named simple max-stable process (Ribatet, 2017; Ribatet et al., 2016). It has a spectral representation, which is presented by De Haan (1984) as follows

$$X(s) = \bigvee_{i=1}^{\infty} \zeta_i Y_i(s), \; s \in \mathcal{S} \tag{3}$$

where $\zeta_i, i \geq 1$ is a Poisson point process on $\mathbb{R}^+$ with intensity $\zeta^{-2} d\zeta$ and the $Y_i(s), i \geq 1$ are independent copies of a stochastic process $Y(s) \geq 0$ with

$\mathbb{E}[Y(s)] = 1$.
The multivariate max-stable model for any set of m spatial locations $\mathbf{S} = \{s_1, \cdots, s_m\} \subset \mathcal{S}$, is given by

$$\mathbb{P}\big\{X(s_1) \leq x_1, \cdots, X(s_m) \leq x_m\big\} = \exp\big\{-V_{\mathbf{S}}(x_1, \cdots, x_m)\big\} \tag{4}$$

where

$$V_{\mathbf{S}}(x_1, \cdots, x_m) = \mathbb{E}\Big\{\max\Big[\frac{Y(s_1)}{x_1}, \cdots, \frac{Y(s_m)}{x_m}\Big]\Big\}, \tag{5}$$

is called the exponent measure that satisfies homogeneity of order -1, i.e $V_{\mathbf{S}}(bx_1, \cdots, bx_m) = b^{-1}V_{\mathbf{S}}(x_1, \cdots, x_m)$, $b > 0$.
Various max-stable models were presented, and each has an explicit formula for the exponent measure according to the choice of the process $Y(s)$, for instance, the Smith model (Smith, 1990), the Schlather model (Schlather, 2002), the Brown-Resnick model (Kabluchko et al., 2009) and the Extremal-t model (Opitz, 2013).
Here, we propose a space-time max-stable model to deal with the issue of temporal nonstationarity in spatial extremal dependence. The idea of the model is to mix two max-stable models, with mixing proportion varying over time. Let $X^1(s)$ and $X^2(s)$ be two independent simple max-stable processes defined on the same space $\mathcal{S}$. For any $\pi(t) \in [0, 1]$, and $t = 1, \cdots, T$, consider the spatio-temporal process:

$$X(s, t) = \max\big\{\pi(t)X^1(s), (1 - \pi(t))X^2(s)\big\}. \tag{6}$$

It is a simple space-time max-stable process with bivariate distribution defined as

$$\mathbb{P}\big(X(s, t) \leq x_1, X(s', t) \leq x_2\big) = \exp\Big\{-V^{mix}_{\mathbf{S},t}(x_1, x_2)\Big\}$$

with

$$V^{mix}_{\mathbf{S},t}(x_1, x_2) = \pi(t)V^1_{\mathbf{S}}(x_1, x_2) + (1 - \pi(t))V^2_{\mathbf{S}}(x_1, x_2), \tag{7}$$

it is the exponent function for the time-varying max-stable mixture model, it summarizes the extremal dependence of $X(s)$ and $X(s')$ at time t. In (7), $\mathbf{S} = \{s, s'\}$, V^1 and V^2 denote the exponent measures of $X^1(s)$ and $X^2(s)$ respectively, and $\pi(t)$ is a temporaly varying proportion, which determines which of the processes $X^1(s)$ and $X^2(s)$ is dominant at time t.
Figure 1 shows a realization of such a process on a regular 50×50 grid over the $[0, 1]^2$. The first mixing component is an Extremal-t process with

degree of freedom equals to 5 and exponential correlation function $\rho(h) = \exp(-\|h\|/\phi_1)$, with range $\phi_1 = 0.6$, the second one is an isotropic Smith process with covariance matrix $\Sigma = \phi_2 \, \mathrm{Id}_2$, $\phi_2 = 0.4$. Twelve time points are considered and the mixing proportion has a linear trend with $\pi(t_1) = 0$ and $\pi(t_{12}) = 1$.

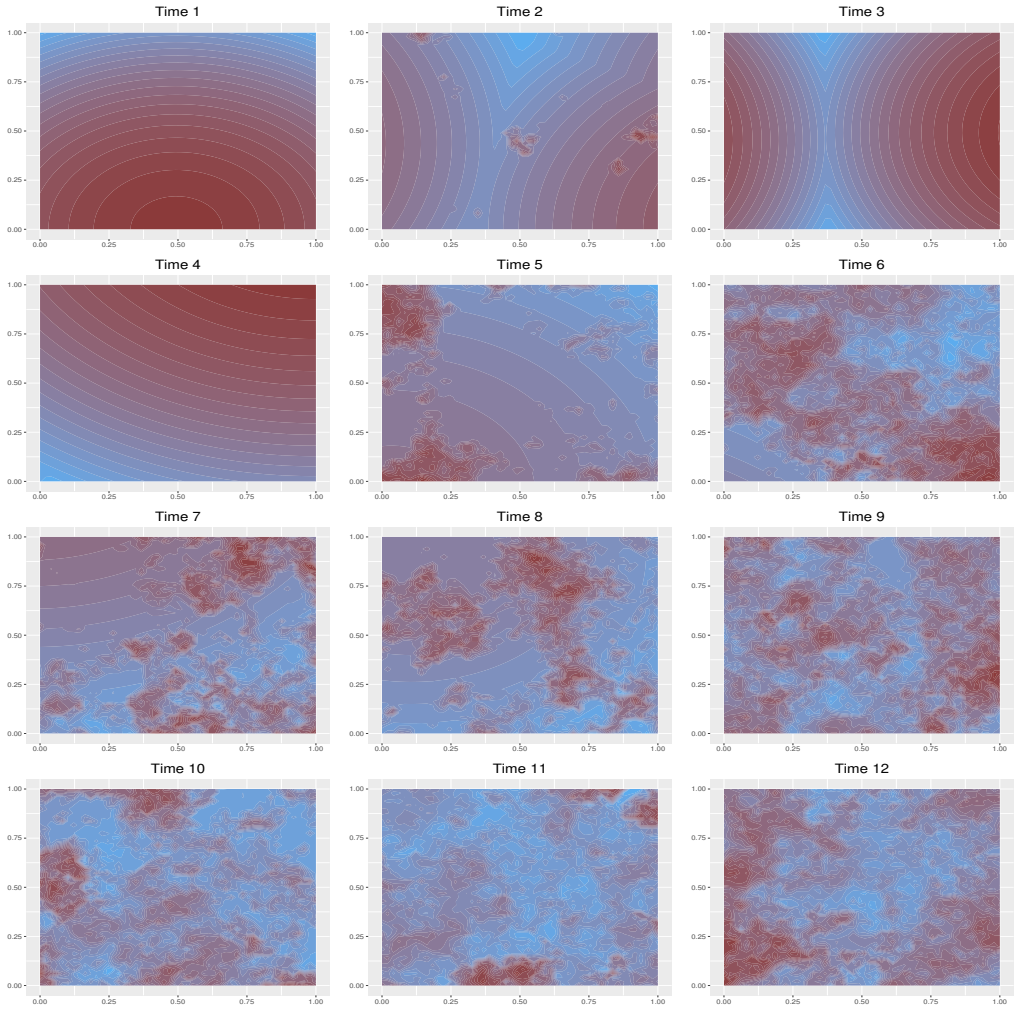

Figure 1: Realization of a time-varying max-stable mixture process on logarithm scale for twelve-time points. Here, an Extremal-t process with degree of freedom equals 5 and exponential correlation function $\rho(h) = \exp(-\|h\|/\phi_1)$, $\phi_1 = 0.6$, is mixed with an isotropic Smith process with a covariance matrix $\Sigma = \phi_2 \, \mathrm{Id}_2$, $\phi_2 = 0.4$. The mixing proportion has a linear trend, with $\pi(t_1) = 0$ and $\pi(t_{12}) = 1$.

If $\pi(t)$ is constant over time, then the prosess is temporaly stationary. On the contrary, if $\pi(t)$ depends on time, the model is non stationary in time. For example, one could consider $\text{logit}\{\pi(t)\} = Y_t^T\beta$ where Y_t is a vector of covariates at time t and β represents its associated vector of parameters. It is worth mentioning that the logit function is used to ensure that $\pi(t)$ remains between 0 and 1.
The definition of the model makes it flexible and may be more suitable for modeling environmental events under climate change. It accommodates the state of change from one model to another with time and allows using any function for the mixing proportion (linear or nonlinear).

2.1. Measures of extremal dependence

In this subsection, we present two measures of extremal dependence for the proposed model: Extremal coefficient function and F-madogram.

2.1.1. Time-varying extremal coefficient function

The extremal coefficient function captures information about the strength of the extremal dependence for stationary max-stable processes (Schlather and Tawn, 2003). Let $X(s)$ and $X(s')$ be simple max-stable processes at locations s and s' respectively, let $h = s - s'$ be the spatial lag. The extremal coefficient function $\theta(h)$ is

$$\theta(h) = -x \log \mathbb{P}\big\{X(s) \leq x, X(s') \leq x\big\} = V_{\mathbf{S}}(1,1) \tag{8}$$

The extremal coefficient takes values in $[1,2]$, $\theta(h) = 1$ when $X(s)$ and $X(s')$ are completely dependent, while $\theta(h) = 2$ when they are independent. For each max-stable model, there is a theoretical formula for the extremal coefficient as a function of the spatial lag h (Ribatet, 2013).
Below, we calculate the extremal coefficient $\theta^{mix}(h,t)$ for the time-varying max-stable mixture model. It depends on the spatial lag h and the time point $t \in \mathcal{T}$, it may capture changes in the extremal dependence over time.

Proposition 1. *Let $\{X^1(s), s \in \mathcal{S}\}$ and $\{X^2(s), s \in \mathcal{S}\}$ be two simple max-stable processes with extremal coefficient function $\theta^1(h)$ and $\theta^2(h)$, respectively, let $\pi(t) \in [0,1]$, $t \in \mathcal{T}$. Then, at any time point $t \in \mathcal{T}$ and any spatial lag $h = s - s'$, $s, s' \in \mathcal{S}$, the extremal coefficient of the time-varying max-stable mixture process $\{X(s,t), s \in \mathcal{S}, t \in \mathcal{T}\}$ defined by (6), is given by*

$$\theta^{mix}(h,t) = \pi(t)\theta^1(h) + (1 - \pi(t))\theta^2(h). \tag{9}$$

Proof of Proposition 1. Recall that, the exponent measures $V_{\mathbf{S}}$ for any max-stable process is homogeneous of order -1, and $V^1_{\mathbf{S}}(1,1) = \theta^1(h)$, $V^2_{\mathbf{S}}(1,1) = \theta^2(h)$, respectively. Since at each time point t, the spatial process is stationary, we have for any x, using (7)

$$\begin{aligned}\theta^{mix}(h,t) &= V^{mix}_{\mathbf{S},t}(1,1)\\ &= \pi(t)V^1_{\mathbf{S}}(1,1) + (1-\pi(t))V^2_{\mathbf{S}}(1,1)\\ &= \pi(t)\theta^1(h) + (1-\pi(t))\theta^2(h),\end{aligned}$$

which is the announced result. □

Figure 2 represents a surface plot for the extremal coefficient of the process shown in Figure 1. It shows the temporal evaluation for the spatial extremal coefficient. For display purposes, we considered twelve distances of equal length, from 0 to the maximum pairwise distance of 1.414.

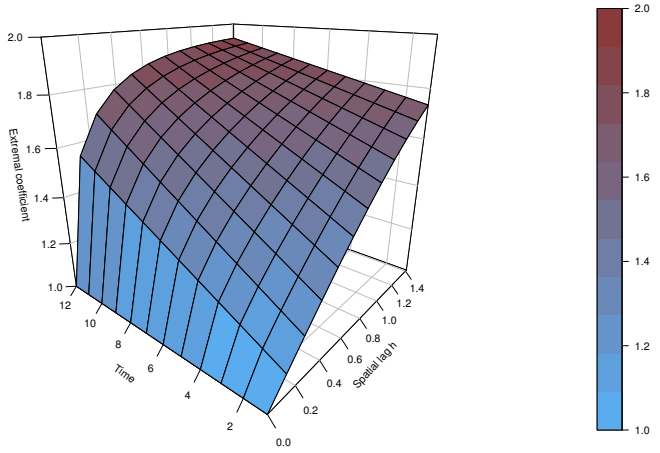

Figure 2: Surface plot for the extremal coefficient of the process which is shown in Figure 1.

2.1.2. Time-varying spatial F-madogram

Cooley et al. (2006) proposed the F-madogram as a measure of spatial extremal dependence for stationary spatial max-stable processes with unit Fréchet margins. It is defined as

$$\mathcal{V}_F(h) = \frac{1}{2}\mathbb{E}\Big[\big|F(X(s)) - F(X(s'))\big|\Big] \tag{10}$$

where $F(X(s))$ and $F(X(s'))$ are the marginal distributions function of $X(s)$ and $X(s')$, respectively, and h refers to the spatial lag between the locations s and s'. We have $\mathcal{V}_F(h) \in [0, \frac{1}{6}]$, where 0 ocurs if $X(s)$ and $X(s')$ that are completely dependent and $\frac{1}{6}$ occurs if to they are independent.
The F-madogram has a strong link with the extremal coefficient:

$$\mathcal{V}_F(h) = \frac{1}{2} - \frac{1}{\theta(h)+1} \tag{11}$$

For more detail about the theoretical properties of F-madogram, we refer to Cooley et al. (2006) and Naveau et al. (2009).
As a consequence, the F-madogram of the time-varying max-stable mixture process $\{X(s,t), s \in \mathcal{S}, t \in \mathcal{T}\}$ define by (6) is given by:

$$\mathcal{V}_F^{mix}(h,t) = \frac{1}{2} - \frac{1}{\theta^{mix}(h,t)+1} \tag{12}$$

where $\mathcal{V}_F^{mix}(h,t) \in [0, \frac{1}{6}]$ and $\theta^{mix}(h,t) = \pi(t)\theta^1(h) + (1-\pi(t))\theta^2(h)$
The surface plot for the F-madogram of the process which shown in Figure 1 is presented in Figure 3. It shows the temporal evolution of the spatial F-madogram. We consider twelve distances as in Figure 2.

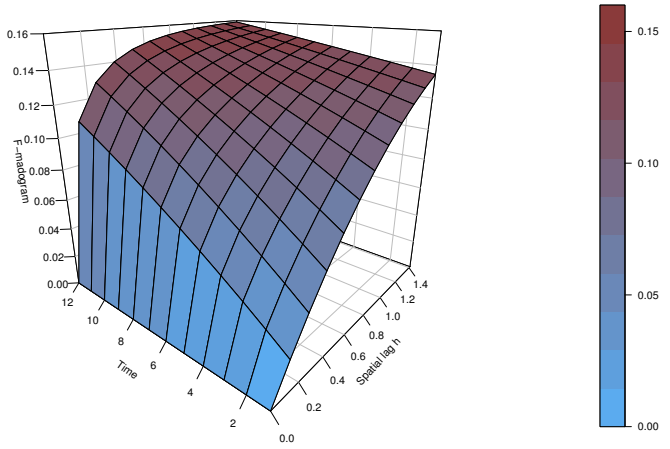

Figure 3: Surface plot for the F-madogram of the process which is shown in Figure 1.

3. Statistical inference

3.1. Maximum composite likelihood estimator (MCLE)

Owing to the computational intractable issues of the full likelihood inference for max-stable models, the Maximum composite likelihood estimator (MCLE) is the standard inference approach nowadays for these models (Lindsay, 1988; Padoan et al., 2010; Varin et al., 2011; Castruccio et al., 2016; Huser et al., 2019). Consider a parametric form for $\pi(t)$, e.g. $\pi(t) = at + b$ and let us denote by Ψ the vector of the parameters of our spatio-temporal model, then the MCLE can be defined as

$$\hat{\Psi} = \arg\max \mathcal{P}(\Psi) \tag{13}$$

where

$$\mathcal{P}(\Psi) = \sum_{t=1}^{T} \sum_{j=1}^{m-1} \sum_{j'=j+1}^{m} \mathcal{W}_{jj'} \log f(x_{tj}, x_{tj'}; \Psi) \tag{14}$$

with T is the number of time points, m is the number of locations, f is the bivariate density function associated with the model defined in (6), and $\mathcal{W}_{jj'} \geq 0$ are weights that specify the contributions of each pair.
Under some regularity conditions, satisfied for standard max-stable models, $\hat{\Psi}$ is strongly consistent and asymptotically normal distributed (Padoan et al., 2010; Davison and Gholamrezaee, 2012)

$$\hat{\Psi} \xrightarrow{\mathcal{D}} \mathcal{N}(\Psi, \mathcal{H}(\Psi)^{-1}\, \mathcal{J}(\Psi)\, \mathcal{H}(\Psi)^{-1}) \quad \text{as } T \to \infty. \tag{15}$$

where $\mathcal{H}(\Psi) = \mathbb{E}\big[-\nabla^2 \mathcal{P}(\Psi)\big]$ is named the sensitivity matrix and $\mathcal{J}(\Psi) = \mathbb{V}\big[\nabla \mathcal{P}(\Psi)\big]$ is named the variability matrix. By estimating the matrices $\mathcal{H}(\Psi)$ and $\mathcal{J}(\Psi)$, one can assess the variance of the estimated parameters.

3.2. Model selection

The model selection criterion that is associated with the MCLE is the Composite Likelihood Information Criterion (CLIC) (Varin and Vidoni, 2005)

$$\text{CLIC} = -2\,\mathcal{P}(\hat{\Psi}) + 2\,\text{tr}(\hat{\mathcal{H}}(\hat{\Psi})^{-1}\, \hat{\mathcal{J}}(\hat{\Psi})) \tag{16}$$

where $\hat{\Psi}$ is the vector of the estimated parameters using MCLE, tr is the trace of a matrix, $\hat{\mathcal{H}}(\hat{\Psi})$ and $\hat{\mathcal{J}}(\hat{\Psi})$ are the empirical estimations of the sensitivity matrix and variability matrix, respectively, which are defined by

$$\hat{\mathcal{H}}(\hat{\Psi}) = -\sum_{t=1}^{T} \sum_{j=1}^{m-1} \sum_{j'=j+1}^{m} \mathcal{W}_{jj'} \frac{\partial^2 \log f(x_{tj}, x_{tj'}; \hat{\Psi})}{\partial \Psi \partial \Psi^\intercal} \tag{17}$$

and

$$\hat{\mathcal{J}}(\hat{\Psi}) = \sum_{t=1}^{T} \left\{ \sum_{j=1}^{m-1} \sum_{j'=j+1}^{m} \mathcal{W}_{jj'} \frac{\partial \log f(x_{tj}, x_{tj'}; \hat{\Psi})}{\partial \Psi} \right\} \times \left\{ \sum_{j=1}^{m-1} \sum_{j'=j+1}^{m} \mathcal{W}_{jj'} \frac{\partial \log f(x_{tj}, x_{tj'}; \hat{\Psi})}{\partial \Psi} \right\}^{\intercal} \tag{18}$$

For comparison among different models, the lowest value of CLIC indicates the best-fitting model.

4. Simulation study

In this section, we first assess the performance of the maximum composite likelihood estimator (13) to estimate the parameters of our proposed model (6). We assume that the time-varying mixing proportion $\pi(t)$ has a linear trend over time. To ensure that the mixing proportion remains between 0 and 1 and to avoid the use of any transformation functions (such as logit, probit, etc.), we express the mixing proportion at any time t as:

$$\pi(t) = \pi_B + (t - t_B) * \frac{\pi_E - \pi_B}{t_E - t_B} \tag{19}$$

where π_B and π_E are the mixing proportions at the beginning and the end of the time, respectively. The term $\frac{\pi_E - \pi_B}{t_E - t_B}$ gives the slope of the linear trend of the mixing proportion.
Depending on the considered time-varying mixing proportion $\pi(t)$ (19), and assuming we have n time observations of the process $(t_1, \cdots, t_n \in [t_B, t_E])$, we propose a Z-test statistic derived from the central limit theorem for the MCLE with the aim of validation the trend in the mixing proportion. For this purpose, we consider testing $H_0 : \pi_B = \pi_E$ against $H_1 : \pi_B \neq \pi_E$, the test statistic is defined as

$$Z_{\pi_B, \pi_E} = \frac{\hat{\pi}_B - \hat{\pi}_E}{\sqrt{\widehat{Var}(\hat{\pi}_B) + \widehat{Var}(\hat{\pi}_E) - 2\widehat{Cov}(\hat{\pi}_B, \hat{\pi}_E)}} \xrightarrow{\mathcal{D}} \mathcal{N}(0, 1) \quad \text{as } n \to \infty. \tag{20}$$

For that, the second matter in this section is to assess the performance of the proposed test statistic.
Throughout this section, we consider two time-varying max-stable mixture

models defined in (6), assuming that the mixing proportion $\pi(t)$ as in (19). The details of the considered models are below, where Ψ is the vector that gathers the model parameters that will be estimated.

- I: It combines a Brown-Resnick model with semivariogram $\gamma(h) = (\|h\|/\phi_1)^{\alpha_1}$, $\phi_1 > 0$, $0 < \alpha_1 \leq 2$ and an Isotropic Smith model with a covariance matrix $\Sigma = \phi_2 \, \mathrm{Id}_2$. The model parameters are $\Psi = \{\pi_B, \pi_E, \phi_1, \alpha_1, \phi_2\}^\intercal$.

- II: It combines an Extremal-t model with a Gaussian correlation functions $\rho(h) = \exp(-(\|h\|/\phi_1)^2)$, $\phi_1 > 0$, which a has degree of freedom $df_1 \geq 1$ and an Extremal-t model with an exponential correlation functions $\rho(h) = \exp(-\|h\|/\phi_2)$, $\phi_2 > 0$, which a has degree of freedom $df_2 \geq 1$. The model parameters are $\Psi = \{\pi_B, \pi_E, \phi_1, df_1, \phi_2, df_2\}^\intercal$.

4.1. Setup of the simulation

We consider that the size of the simulated data from models I and II should be close to the size of the data in the application section (see Section 5). Therefore, we fixed the number of locations $m = 40$ and consider $T = 50$ time points. The coordinates of these locations are generated randomly and uniformly over $[0, 1]^2$. The simulations are carried out using the function *rmaxstab* of the `R` package SpatialExtremes (Ribatet, 2022). We consider several parameters for the time-varying mixing proportions π_B and π_E. The parameters of model I are fixed to $\phi_1 = 0.2$, $\alpha_1 = 1$, and $\phi_2 = 0.7$, while the parameters of model II are fixed to $\phi_1 = 0.4$, $df_1 = 2$, $\phi_2 = 0.1$, and $df_2 = 6$. The simulations for each model are repeated 200 times in order to compute the empirical performance metrics.

4.2. Performance of MCLE

To assess the efficiency of the maximum composite likelihood estimator (MCLE) to estimate the parameters of our proposed model, we investigate its ability to recover the true parameters of the two simulated models, I and II. We consider several parameters of the time-varying mixing proportion $(\pi_B, \pi_E) \in \{(0, 1), (0.2, 0.9), (0.5, 0), (0.8, 0.6)\}$. For each, we used (13) assuming equal weights to estimate the parameters. Then, we created boxplots of the errors of the estimated parameters $(\hat{\Psi} - \Psi)$ for models I and II as shown in Figure 4 and Figure 5, respectively. Also, we computed the per-

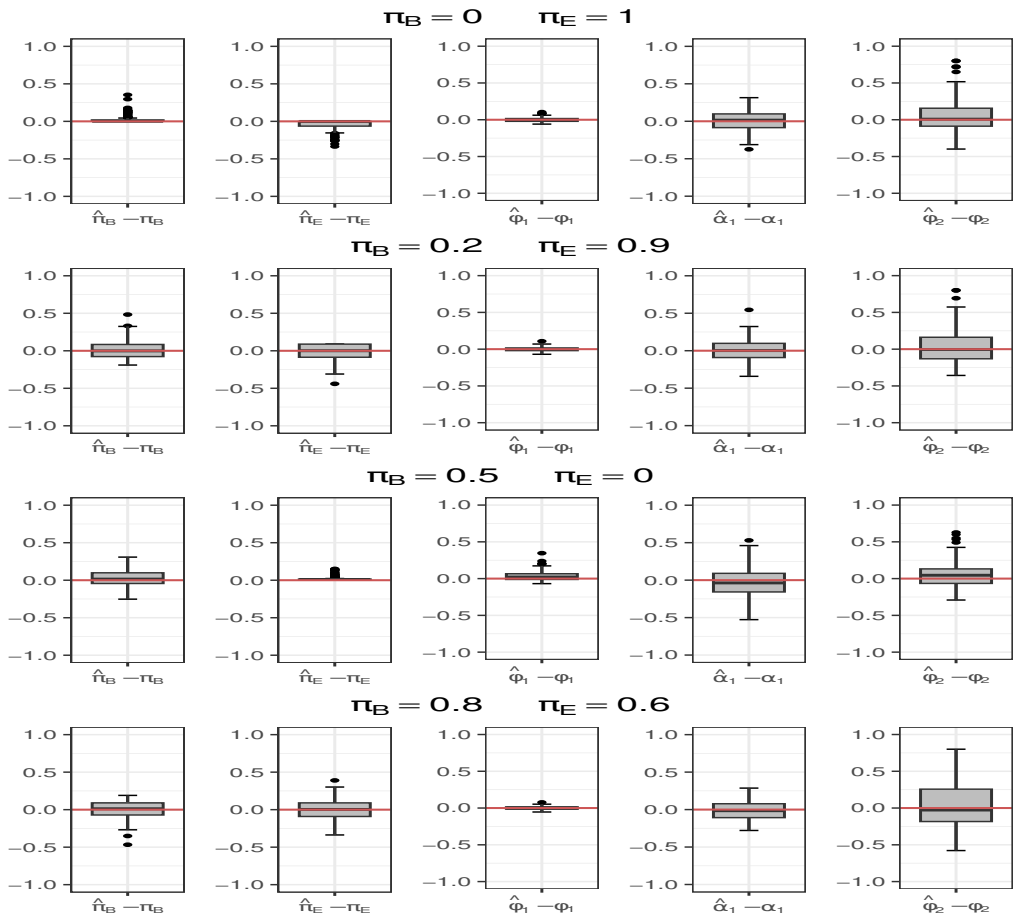

Figure 4: Boxplots display $(\hat{\Psi} - \Psi)$ of the estimated parameters vector $\hat{\Psi} = \{\hat{\pi}_B, \hat{\pi}_E, \hat{\phi}_1, \hat{\alpha}_1, \hat{\phi}_2\}^\intercal$ of the model I by MCLE. The true values of the parameters are $\phi_1 = 0.2$, $\alpha_1 = 1$, $\phi_2 = 0.7$, and $(\pi_B, \pi_E) \in \{(0,1), (0.2, 0.9), (0.5, 0), (0.8, 0.6)\}$. The number of simulations equals 200. The red horizontal line shows the zero value.

formance metrics: the mean estimate, the root mean square error (RMSE), and the mean absolute error (MAE) as follows

$$\text{RMSE} = \sqrt{N^{-1}\sum_{i=1}^{N}(\hat{\Psi}_i - \Psi)^2} \quad \text{and} \quad \text{MAE} = N^{-1}\sum_{i=1}^{N}|\hat{\Psi}_i - \Psi| \tag{21}$$

where N is the number of simulations and $\hat{\Psi}_i$ is the ith estimation. The performance metrics of the MCLE for models I and II are displayed in Table

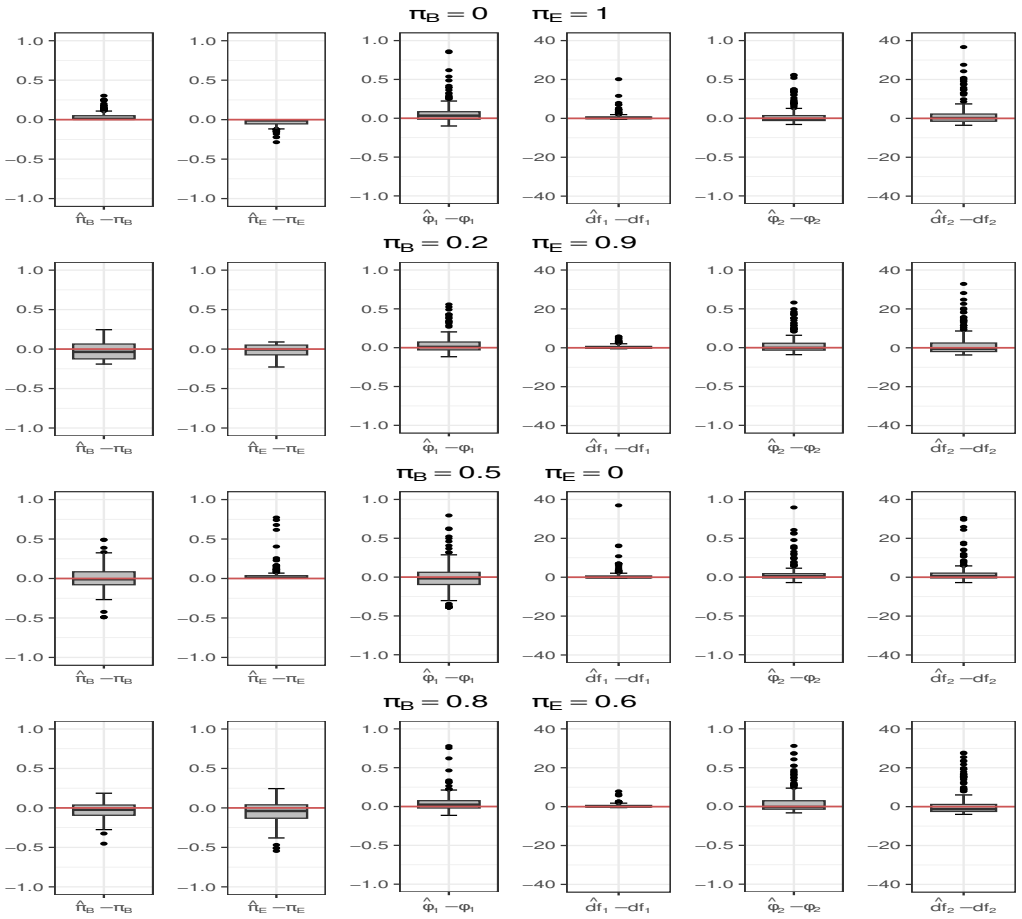

Figure 5: Boxplots display $(\hat{\Psi} - \Psi)$ of the estimated parameters vector $\hat{\Psi} = \{\hat{\pi}_B, \hat{\pi}_E, \hat{\phi}_1, \hat{df}_1, \hat{\phi}_2, \hat{df}_2\}^\intercal$ of the model II by MCLE. The true values of the parameters are $\phi_1 = 0.4$, $df_1 = 2$, $\phi_2 = 0.1$, $df_2 = 6$, and $(\pi_B, \pi_E) \in \{(0,1), (0.2, 0.9), (0.5, 0), (0.8, 0.6)\}$. The number of simulations equals 200. The red horizontal line shows the zero value.

1 and Table 2, respectively. Regarding model I, Figure 4 shows that MCLE works well in all cases. The parameters are well estimated, without large variances except for ϕ_2, which has a relatively large variance. The medians of the errors in the estimations are equal to zero in most cases, indicating good performance. Furthermore, the estimates are unbiased, as the mean estimates are approximately equal to the true values, as explained in Table 1. Also, the estimation of ϕ_2 is always less accurate than the estimations of ϕ_1 and α_1 (the RMSE and MAE are higher), this accuracy decreases when

Table 1: The mean estimate, RMSE, and MAE of the maximum composite likelihood estimator (MCLE) for 200 simulations of model I with parameters $\phi_1 = 0.2$, $\alpha_1 = 1$, $\phi_2 = 0.7$, and $(\pi_B, \pi_E) \in \{(0,1), (0.2, 0.9), (0.5, 0), (0.8, 0.6)\}$.

	Performance metrics of MCLE		
True parameters	Mean estimate	RMSE	MAE
$\pi_B = 0$	0.024	0.057	0.024
$\pi_E = 1$	0.956	0.083	0.044
$\phi_1 = 0.2$	0.199	0.029	0.023
$\alpha_1 = 1$	1.010	0.133	0.107
$\phi_2 = 0.7$	0.746	0.207	0.150
$\pi_B = 0.2$	0.209	0.118	0.094
$\pi_E = 0.9$	0.880	0.108	0.086
$\phi_1 = 0.2$	0.200	0.028	0.023
$\alpha_1 = 1$	1.003	0.137	0.109
$\phi_2 = 0.7$	0.732	0.222	0.172
$\pi_B = 0.5$	0.533	0.107	0.082
$\pi_E = 0$	0.023	0.037	0.023
$\phi_1 = 0.2$	0.230	0.067	0.048
$\alpha_1 = 1$	0.970	0.193	0.154
$\phi_2 = 0.7$	0.755	0.171	0.127
$\pi_B = 0.8$	0.802	0.120	0.095
$\pi_E = 0.6$	0.602	0.137	0.111
$\phi_1 = 0.2$	0.201	0.021	0.017
$\alpha_1 = 1$	0.994	0.119	0.099
$\phi_2 = 0.7$	0.759	0.334	0.260

the mixing proportion for the first mixing model remains higher than the second mixing model with time (case when $\pi_B = 0.8$ and $\pi_E = 0.6$). From the results of MCLE for the parameters of model II in Figure 5, the medians of the errors in the estimates are near zero. However, there are some outliers, especially in the estimations of the parameters of the second mixing model ϕ_2 and df_2. In general, despite the complexity of the model, the results are satisfactory without any strong bias as explained in the mean estimate metric in Table 2. Also, the estimation of ϕ_2 and df_2 is less accurate than

Table 2: The mean estimate, RMSE, and MAE of the maximum composite likelihood estimator (MCLE) for 200 simulations of model II with parameters $\phi_1 = 0.4$, $df_1 = 2$, $\phi_2 = 0.1$, $df_2 = 6$, and $(\pi_B, \pi_E) \in \{(0,1), (0.2, 0.9), (0.5, 0), (0.8, 0.6)\}$.

	Performance metrics of MCLE		
True parameters	Mean estimate	RMSE	MAE
$\pi_B = 0$	0.040	0.069	0.040
$\pi_E = 1$	0.961	0.061	0.039
$\phi_1 = 0.4$	0.470	0.169	0.089
$df_1 = 2$	2.720	2.179	0.923
$\phi_2 = 0.1$	0.131	0.116	0.063
$df_2 = 6$	8.026	6.472	3.466
$\pi_B = 0.2$	0.169	0.119	0.102
$\pi_E = 0.9$	0.884	0.083	0.068
$\phi_1 = 0.4$	0.445	0.126	0.077
$df_1 = 2$	2.488	0.134	0.783
$\phi_2 = 0.1$	0.144	0.133	0.077
$df_2 = 6$	7.769	6.451	3.762
$\pi_B = 0.5$	0.502	0.148	0.109
$\pi_E = 0$	0.047	0.117	0.047
$\phi_1 = 0.4$	0.402	0.195	0.128
$df_1 = 2$	2.853	3.503	1.198
$\phi_2 = 0.1$	0.144	0.131	0.061
$df_2 = 6$	7.988	5.325	2.599
$\pi_B = 0.8$	0.767	0.104	0.080
$\pi_E = 0.6$	0.554	0.143	0.109
$\phi_1 = 0.4$	0.453	0.151	0.081
$df_1 = 2$	2.397	1.182	0.639
$\phi_2 = 0.1$	0.163	0.188	0.100
$df_2 = 6$	7.420	7.022	4.215

the estimation of ϕ_1 and df_1 (the RMSE and MAE are higher), this accuracy decreases when the mixing proportion for the first mixing model still the higher for all time points (case when $\pi_B = 0.8$ and $\pi_E = 0.6$), this is similar to what appeared in the results of model I.

4.3. Performance of the proposed test statistic Z_{π_B,π_E}

We investigate the performance of the proposed test statistic Z_{π_B,π_E} in detecting a trend in the mixing proportion. We test whether the null hypothesis $H_0 : \pi_B = \pi_E$ rejects in all the considered cases of π_B and π_E. For each of the considering models I and II, we examine three cases with a true $\pi_B \in \{0.2, 0.5, 0.8\}$. In all cases, a true π_E takes all the values in the set $\{0, 0.1, \cdots, 1\}$. We compute the empirical power of the test, i.e. empirical probability of rejecting H_0, based on 200 simulations. We test the hypothesis at three significance levels $\alpha \in \{0.1, 0.05, 0.01\}$. The results concerning models I and II are summarized in Figure 6 and Figure 7, respectively. In

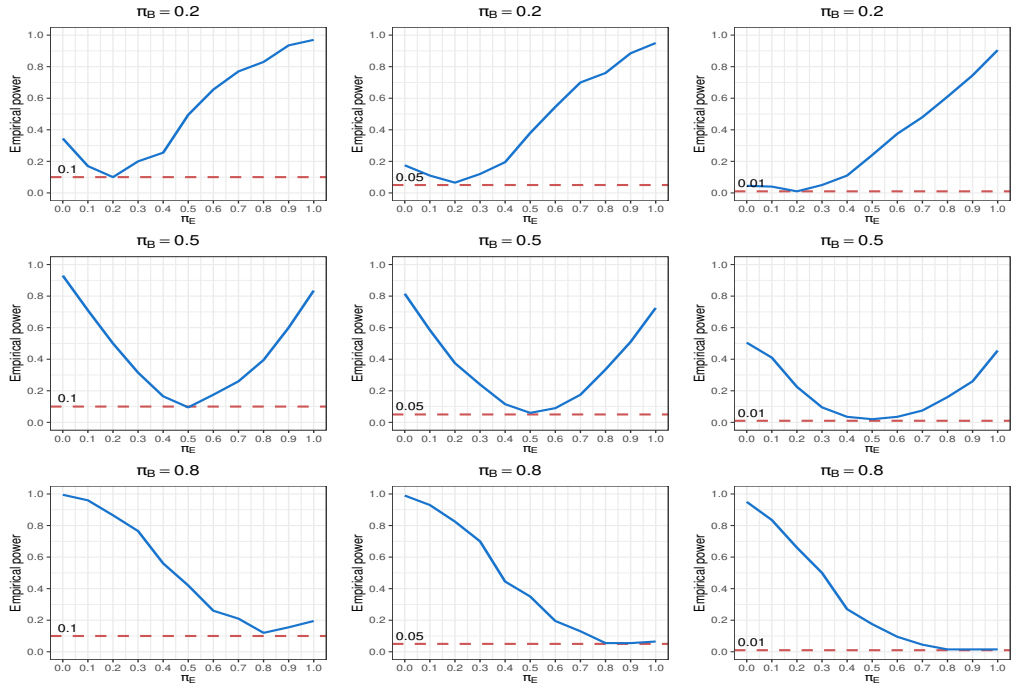

Figure 6: Empirical power of the test, based on 200 simulations of the model I with $\phi_1 = 0.2$, $\alpha_1 = 1$, $\phi_2 = 0.7$, π_B is 0.2,0.5 and 0.8 (for the top row, middle row, and bottom row respectively) and $\pi_E \in \{0, 0.1, \cdots, 1\}$. The red horizontal dashed lines represent the significance level $\alpha = 0.1, 0.05, 0.01$.

general, the results show that the performance of the proposed statistic is satisfactory. The test is unbiased (the empirical power greater than α). Also, the empirical power of the test is higher at $\alpha = 0.1$, which suggests that we have a good chance of correctly rejecting the null hypothesis when it is false.

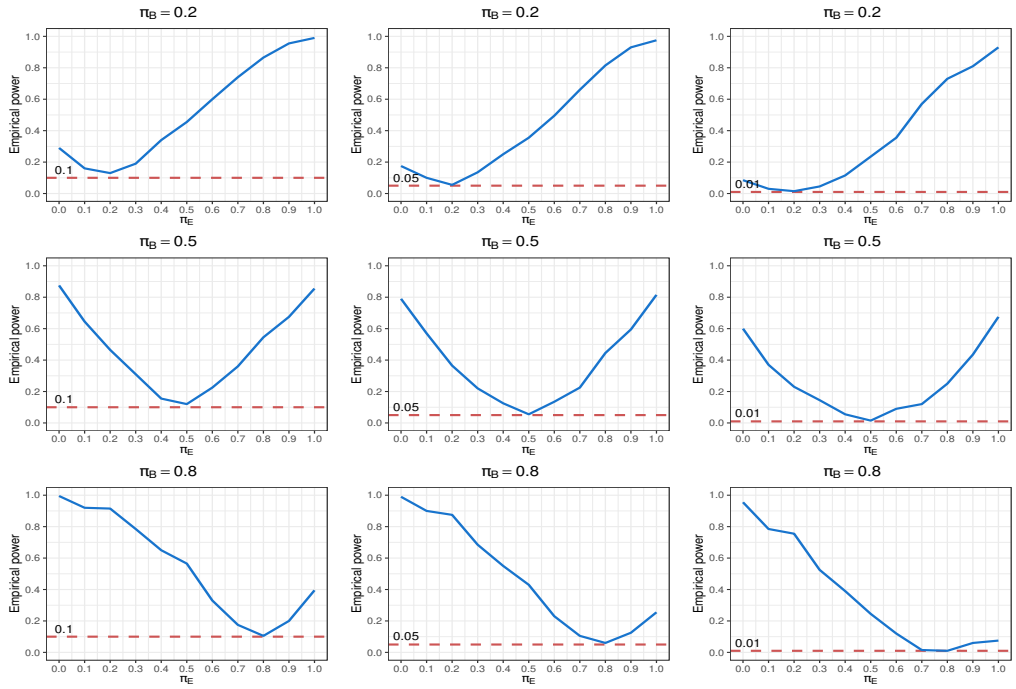

Figure 7: Empirical power of the test, based on 200 simulations of the model II with $\phi_1 = 0.4$, $df_1 = 2$, $\phi_2 = 0.1$, $df_2 = 6$, π_B is 0.2,0.5 and 0.8 (for the top row, middle row, and bottom row respectively) and $\pi_E \in \{0, 0.1, \cdots, 1\}$. The red horizontal dashed lines represent the significance level $\alpha = 0.1, 0.05, 0.01$.

It means our test is good at detecting the trend in the mixing proportion when it exists, even at this slightly higher significance level.

5. Rainfall over the south of France

This section is devoted to studying the effect of climate change on the dependence structure of rainfall in the south of France.

5.1. Data set description

Our data represents daily precipitation levels measured by millimeters and recorded at 40 monitoring stations located in the south of France. The distances between the stations range approximately from 21 km to 696 km. The data covered the rainfall period (September-November) through the time duration 1970-2023, so each station has 91*54=4914 observations. It was supplied by Météo-France with high quality, with no missing data. Figure 8

shows the study area and the geographic locations of the monitoring stations. To explore the raw data, Figure 9 displays the daily precipitation levels for

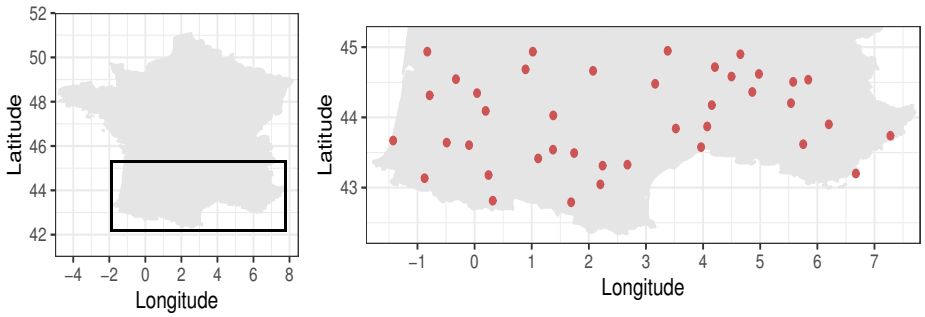

Figure 8: Left panel: France map; the black rectangle determines the studied area (south of France). Right panel: zoom in on the studied area showing the geographical locations of 40 monitoring stations.

September, October, and November through the last 20 years (2004-2023) recorded at four stations chosen to be one on the north, east, south, and west of the studied region. The red dots represent the autumnal precipitation maxima. Visually, it is hard to detect a time trend in the time series from year to year, and this is suitable for our assumption that there is no trend in the marginal distribution. Furthermore, the maxima appear somewhat scattered, which means there is no shifting in the date of occurrence of the maximum precipitation level within autumn over the years. However, from these exploratory plots, it is unclear whether the spatial dependence of precipitation changes with time or not, where we will see that in the following subsections.

5.2. Workflow of Modeling

In this work, we consider the autumnal maxima of the daily rainfall, for that maxima are taken over 91 days of each season, resulting in 54 blocks. Generalized Extreme Value distribution (GEV) was fitted to each location separately using a Maximum Likelihood Estimator (MLE). We assessed the goodness of fit using the Kolmogorov-Smirnov test per location, where it exhibited a good fit with a mean p-value of 0.858. That indicates the marginal distributions are compatible with the max-stable processes, similar to what was found by Oesting and Naveau (2020), where they studied the same area.

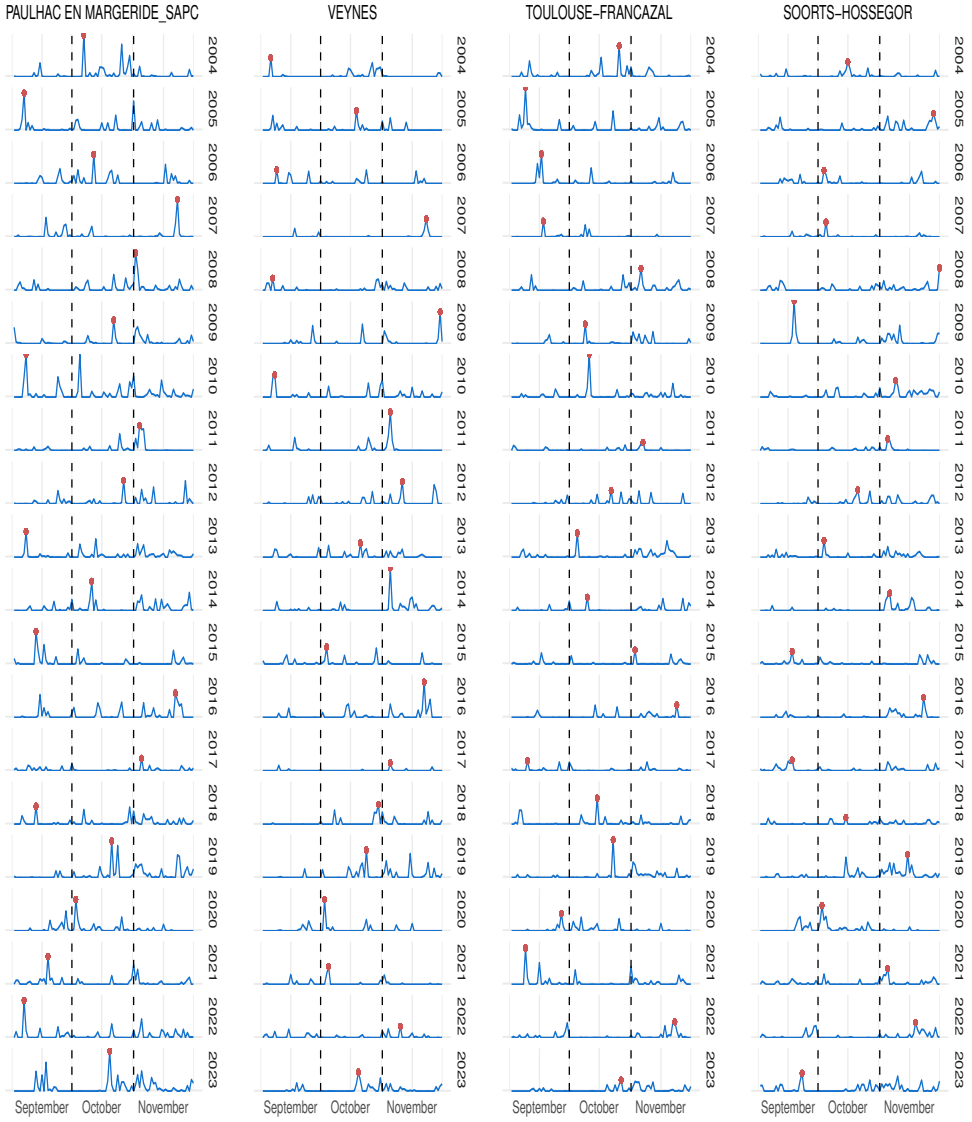

Figure 9: Daily rainfall recorded at four stations for September, October, and November per Autumn 2004-2023 in the solid blue curves. The red dots represent the Autumnal rainfall maxima. The names of the stations are provided on the top side.

Since we focus on the spatial dependence of $\{X(s), s \in \mathcal{S}\}$ and in order to fit the max-stable models to the maxima, the univariate distributions are transformed to unit Fréchet distributions. In this paper, we used the parametric transformation according to the following formula

$$X(s) \to \frac{-1}{\log\Big\{F\big[X(s); \mu(s), \sigma(s), \xi(s)\big]\Big\}} \tag{22}$$

where $F\big[.; \mu(s), \sigma(s), \xi(s)\big]$ is the GEV cumulative distribution function with parameters $\mu(s)$, $\sigma(s)$ and $\xi(s)$.

To explore the existence of anisotropy spatial extremal dependence, we make a graphical test like in Bacro et al. (2016) and Ahmed et al. (2017). We calculated the empirical F-madogram from the data. Then, we divided the distances according to their direction into four directional sectors: $(-\pi/8, \pi/8]$, $(\pi/8, 3\pi/8]$, $(3\pi/8, 5\pi/8]$ and $(5\pi/8, 7\pi/8]$, where 0, $\pi/4$, $\pi/2$ and $3\pi/4$ represent the north, east, south and west direction, respectively. Afterward, we plotted smooth lines for the empirical F-madogram associated with the distances in each direction with their 95% confidence intervals, as shown in Figure 10. We notice from Figure 10 that the $\hat{\mathcal{V}}_F(h)$ lines have the same behavior, with low location variability, so we can assume that the spatial extremal dependence is anisotropy.

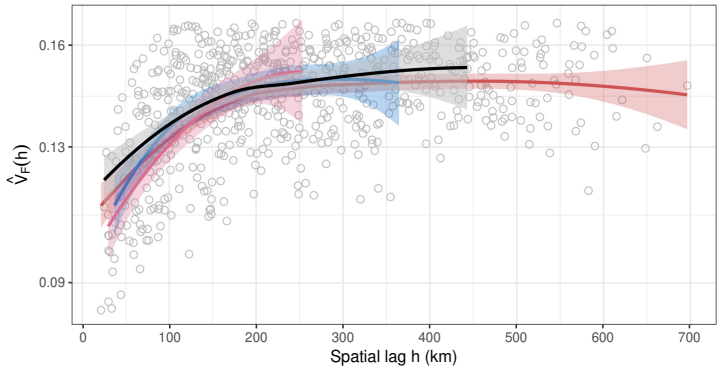

Figure 10: Empirical F-madogram of the autumnal maxima (1970-2023). Gray circles represent the empirical values for all the pairs. The red, blue, pink, and black lines represent the smooth values of the empirical F-madogram using the pairs in the directional sector $(-\pi/8, \pi/8]$, $(\pi/8, 3\pi/8]$, $(3\pi/8, 5\pi/8]$ and $(5\pi/8, 7\pi/8]$, respectively. The shaded bands represent the 95% confidence interval around the smooth lines

In the following subsections, we will proceed to fit several max-stable

models to the autumnal maxima. For comparison purposes later, we begin to fit stationary max-stable models. Then, we will fit stationary max-stable mixture models to determine if they can better represent the extreme dependence structure of the autumnal maxima compared to the stationary max-stable models. After that, a moving time window approach will used as a premier check of the existence of a trend in the mixing proportion. At last, we will fit the proposed time-varying max-stable mixture model. All the models are fitting using MCLE (13) and assuming equal weights.

5.2.1. Fitting stationary max-stable models

We fitted six stationary max-stable models to the rainfall maxima under the assumption of temporal stationarity. The models are described below.

- M1: Isotropic Smith model with a covariance matrix $\Sigma = \phi\,\mathrm{Id}_2$. The model parameter is $\Psi = \phi$.
- M2: Schlather model with an powered exponential correlation function $\rho(h) = \exp(-(\|h\|/\phi)^\alpha)$, $\phi > 0$ and $0 < \alpha \leq 2$. The model parameters are $\Psi = \{\phi, \alpha\}^\intercal$.
- M3: Brown-Resnick model with semivariogram $\gamma(h) = (\|h\|/\phi)^\alpha$, $\phi > 0$ and $0 < \alpha \leq 2$. The model parameters are $\Psi = \{\phi, \alpha\}^\intercal$.
- M4: Extremal-t model with an exponential correlation functions $\rho(h) = \exp(-\|h\|/\phi)$, $\phi > 0$ and degree of freedom $df \geq 1$. The model parameters are $\Psi = \{\phi, df\}^\intercal$.
- M5: Extremal-t model with Whittle-Matérn correlation function $\rho(h) = (2^{1-\alpha}/\Gamma(\alpha))(\|h\|/\phi)^\alpha K_\alpha(\|h\|/\phi)$, $\phi > 0$, $\alpha > 0$ and degree of freedom $df \geq 1$. The model parameters are $\Psi = \{\phi, \alpha, df\}^\intercal$.
- M6: Extremal-t model with Gaussian correlation functions $\rho(h) = \exp(-(\|h\|/\phi)^2)$, $\phi > 0$ and degree of freedom $df \geq 1$. The model parameters are $\Psi = \{\phi, df\}^\intercal$.

The results are summarized in Table 3, where the best-fitting model corresponds to the lowest value of CLIC. Table 3 shows that the Extremal-t model with an exponential correlation function is the best-fitting model in this case.

Table 3: Summary of the fitted stationary max-stable models based on the autumnal maxima of rainfall over south of France. The bold row correspond to the best-fitting model

Models	ϕ	α	df	CLIC
M1	565.673	-	-	362790.8
M2	27.990	1.869	-	364902.2
M3	14.083	0.658	-	362295.1
M4	**119.331**	**-**	**4.903**	**362229.3**
M5	102.141	0.562	4.740	362235.4
M6	67.814	-	3.707	362326.4

5.2.2. Fitting stationary max-stable mixture models

Here, we have fitted three stationary max-stable mixture models. We used the model defined in (6) and kept $\pi(t)$ constant over time. Below is a description of these models.

- MM1: Max-stable mixture model which combine M3 and M1. The model parameters are $\Psi = \{\pi, \phi_1, \alpha_1, \phi_2\}^\intercal$.
- MM2: Max-stable mixture model which combine M6 and M4. The model parameters are $\Psi = \{\pi, \phi_1, df_1, \phi_2, df_2\}^\intercal$.
- MM3: Max-stable mixture model which combine M5 and M6. Note that in model M5, a special case of the whittle-matérn correlation function with $\alpha_1 = 1$ is used. The model parameters are $\Psi = \{\pi, \phi_1, df_1, \phi_2, df_2\}^\intercal$.

Table 4 summarizes the fitting of the models mentioned above, where the subscript indeces 1 and 2 in the estimated parameters refers to the parameters of the first and the second mixing models, respectively. The results show that the best-fitting model is MM2, a mixture between Extremal-t with a Gaussian correlation function and Extremal-t with an exponential correlation function. Additionally, this model provides a more accurate representation of the data than M4, which was the best-fitting model among the max-stable models in Table 3.

Table 4: Summary of the fitted stationary max-stable mixture models based on the autumnal maxima of rainfall over south of France. The bold row correspond to the best-fitting model

Models	π	ϕ_1	α_1	df_1	ϕ_2	df_1	CLIC
MM1	0.485	64.497	1.029	-	188.684	-	362259.5
MM2	**0.230**	**134.627**	**-**	**2.684**	**107.804**	**6.075**	**362222.6**
MM3	0.628	90.358	-	4.389	38.614	6.274	362230.3

5.2.3. Moving time window

In Section 5.2.2, we determined that the max-stable mixture model MM2 was the best fit to represent the extremal dependence of the data under the assumption of temporal stationary. In our proposed model, defined in (6), we allow the mixing proportion $\pi(t)$ to vary with time, resulting in a time-varying extremal dependence. To check for the possibility of the existence of a time-varying extremal dependence, we used an approach based on the data itself, similar to the one used in Nicolet et al. (2016) and Nicolet et al. (2018). This approach motivates us to model a trend in the mixing proportion $\pi(t)$ and provide results that may be comparable with those obtained by fitting our proposed non-stationary model.

Recall that, in Section 5.2.2, we fit the model MM2 for the whole temporal period under study (1970-2023). Here, we need to keep the estimations of the parameters of the two mixing models in MM2 fixed, then re-estimate the mixing proportion π on 21-year moving time windows from (1970-1990) to (2003-2023). For that, we can obtain the extremal coefficient function for each window by applying (9) and using the estimated π for that window. The left panel in Figure 11 displays the temporal evaluation of the estimated mixing proportion considering the 21-year time windows with its uncertainty intervals. It is clear that $\hat{\pi}$ has a negative trend, which enhances the interest in modeling a trend in the mixing proportion. The temporal evaluation of the extremal functions is displayed in the right panel of Figure 11. It shows a positive temporal trend for the extremal function, implying that the extremal dependence decreases in time. For more clarity, we will explain the first and last time windows (1970-1990 and 2003-2023 respectively). For each, we estimate the empirical pairwise extremal coefficient using a madogram-based

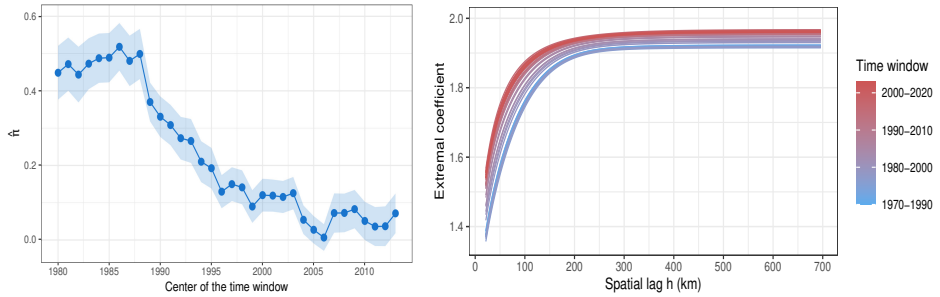

Figure 11: The left panel shows the temporal evaluation of the estimated mixing proportion $\hat{\pi}$ for the model MM2 considering the 21-year time windows from (1970-1990) to (2003-2023) which are represented by the blue dots, where its 95% confidence region showed by the blue shaded area. The X-axis represents the center of the 21-year time window. The right panel displays the temporal evaluation of the extremal functions. The blue curves represent the extremal functions for the oldest time windows, while the red curves represent those for the most recent ones.

approach (Naveau et al., 2009) as follows:

$$\theta(h) = \frac{1 + 2\mathcal{V}_F(h)}{1 - 2\mathcal{V}_F(h)} \tag{23}$$

where $\mathcal{V}_F(h)$ represents the F-madogram defined as in (10). The empirical pairwise extremal coefficient estimates represent the gray points in Figure 12, and the black ones represent the binned estimates (the number of bins equal to 200). Then, using $\hat{\pi}$ and (9), we plot the theoretical extremal function for the model MM2 for each of the two considered windows. It is indicated in Figure 12 by the blue and red curves for the first and the last time windows, respectively. After that, we calculate the range of dependence h_d which is defined as $\theta(h_d) = 1.9$ (Nicolet et al., 2016). For the first window (1970-1990), the value of h_d is 213.94 km, while it is 135.196 km for the last window (2003-2023). That confirms the existence of a negative temporal trend in the extremal dependence.

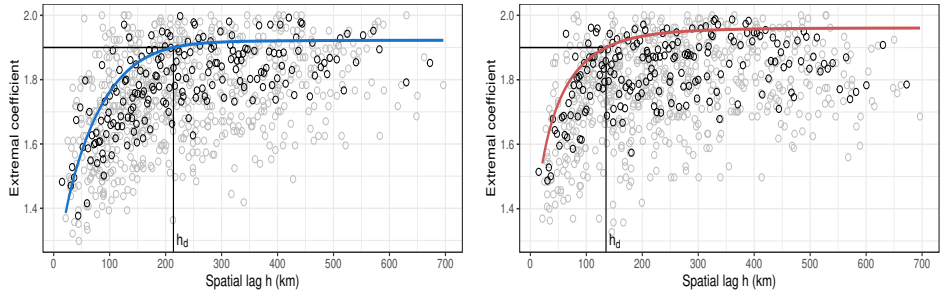

Figure 12: Extremal coefficient function for the first (1970-1990) and the last (2003-2023) windows in the left and right panels, respectively. Gray circles indicate the empirical pairwise estimates of the extremal coefficient; black ones are binned estimates (the number of bins equals 200). The blue and red curves show the theoretical extremal function of the model MM2 for the two considering time windows, respectively. The range of extremal dependence h_d is 213.94 km for the first window and 135.196 km for the last window.

5.2.4. Fitting time-varying max-stable mixture models

Following our results in Section 5.2.3, we fit our model as defined in (6). We assume that $\pi(t)$ has a linear trend as in (19). We consider three different time-varying max-stable mixture models, MMM1-MMM3, described below.

- MMM1: A non-stationary version of the model MM1 (see Section 5.2.2). The model parameters are $\Psi = \{\pi_B, \pi_E, \phi_1, \alpha_1, \phi_2\}^\intercal$.
- MMM2: A non-stationary version of the model MM2 (see Section 5.2.2). The model parameters are $\Psi = \{\pi_B, \pi_E, \phi_1, df_1, \phi_2, df_2\}^\intercal$.
- MMM3: A non-stationary version of the model MM3 (see Section 5.2.2). The model parameters are $\Psi = \{\pi_B, \pi_E, \phi_1, df_1, \phi_2, df_2\}^\intercal$.

The results of fitting the considered models are summarized in Table 5. Recall that, the subscript index 1 and 2 in the estimated parameters refer to the parameters of the first and the second mixing models, respectively. The CLIC value in Table 5 indicates that the best-fitting model for the autumnal maxima of rainfall over the south of France is MMM2. It is a time-varying mixture between the Extremal-t model with a Gaussian correlation function and the Extremal-t model with an exponential correlation function. This result is consistent with the initial check of the data using the moving time windows approach in Section 5.2.3. That is because the best-fitting model MMM2 is the non-stationary version of the model MM2 with a negative linear

Table 5: Summary of the fitted time-varying max-stable mixture models based on the autumnal maxima of rainfall over south of France. The bold row correspond to the best-fitting model

Models	π_B	π_E	ϕ_1	α_1	df_1	ϕ_2	df_1	CLIC
MMM1	0.624	0.263	72.946	1.045	-	202.005	-	362258.9
MMM2	**0.449**	**0.001**	**146.709**	**-**	**2.596**	**106.875**	**6.249**	**362215.8**
MMM3	0.753	0.299	97.708	-	3.829	51.310	7.674	362242.7

trend for the mixing proportion $\pi(t)$. Figure 13 shows the temporal evolutions of the estimated mixing proportion $\hat{\pi}(t)$ and its associate's extremal function for the model MMM2.

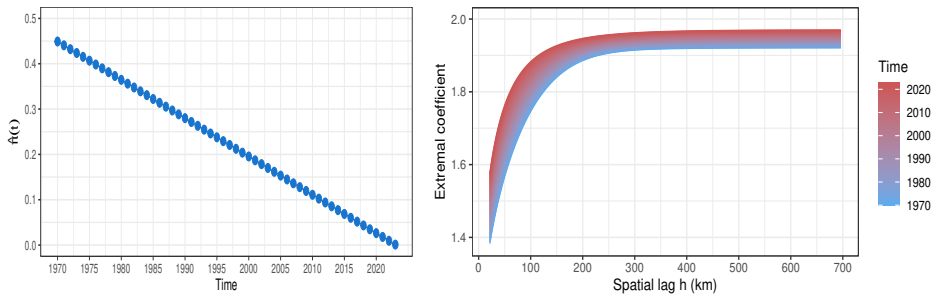

Figure 13: The left panel shows the temporal evaluation of the estimated mixing proportion $\hat{\pi}(t)$ for the model MMM2 considering the time points from 1970 to 2023. The right panel displays the temporal evaluation of the extremal functions for the model MMM2. The blue curves represent the extremal functions for the most ancient time points, while the red curves represent those for the most recent ones.

The left panel of Figure 13 shows that the extremal dependence is represented by a mixture of two models in the early years, while it changes gradually to a single model in the most recent years. As a result, the extremal function exhibits a positive trend over time as can be observed in the right panel of Figure 13. Therefore, the range of extremal dependence decreases in time, as shown in Figure 14. It appears that the range of dependence h_d in 2023 is approximately equal to half its value in 1970, where it changed from 229.05 km to 114.87 km over time. This is relatively consistent with the results obtained by the moving time windows approach.

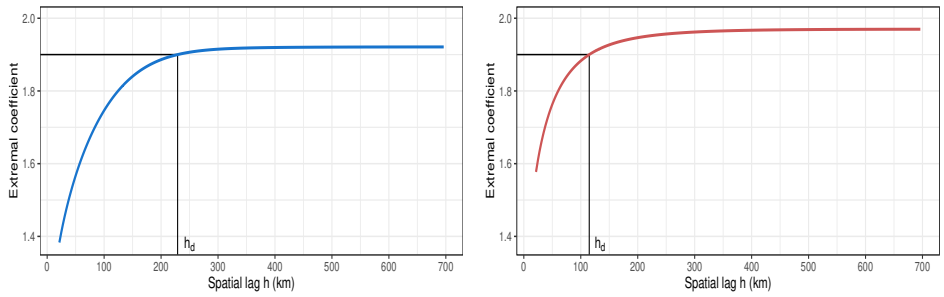

Figure 14: Theoretical extremal functions of the model MMM2 for the first time point (1970) and the last ones (2023) in the left and right panels, respectively. The range of extremal dependence h_d is 229.05 km for the first time point and 114.87 km for the last time point.

It is worth noting that we did additional work to show that our proposed model is better to represent the autumnal maxima of rainfall over the south of France. We fitted the Extremal-t model with an exponential correlation function assuming that the range parameter has a linear trend over time i.e. $\phi(t) = \phi_0 + \lambda t$. The estimations of the parameters are $\phi_0 = 179.14$, $\lambda = -1.9$, and the degree of freedom $df = 5.06$. The CLIC value is 362221.9, which is larger than the CLIC of our proposed mode.
Finally, we consider the best-fitting model MMM2, we perform the proposed statistical test Z_{π_B,π_E} to compare the mixing proportion at the beginning time point π_B with the mixing proportion at the end time point π_E. We test whether the null hypothesis $H_0 : \pi_B = \pi_E$ has to be rejected. We found $|Z_{\pi_B,\pi_E}| = 1.844$ and p-value $= 0.065$. So that, it is reasonnable to consider that there is a linear trend in π ($\pi_B \neq \pi_E$).

6. Discussion and conclusion

The impact of climate change on environmental extreme events makes the existing models, which assume the temporal stationarity of the spatial extremal dependence like max-stable models, not reasonable for modeling such data. In this work, we have addressed this problem by proposing a novel space-time max-stable model, which represents a mixture of two max-stable processes with mixing proportions varying with time. This allows us to model the temporal nonstationarity in the spatial extremal dependence. In particular, we assumed that the mixing proportion is modeled by a function representing a temporal linear trend. We have performed statistical inference

using the maximum composite likelihood (MCLE). Also, we proposed a test statistic to validate the existence of a temporal linear trend in the mixing proportion. The simulation study has shown the efficiency of MCLE in estimating the parameters of the model, and the proposed test statistic performs well even when considering a relatively large significance level ($\alpha = 0.1$).
We have applied the proposed model to study the extreme rainfall in the south of France over the period (1970-2023), to investigate the impact of climate change on its spatial extremal dependence. Various models have been fitted to the data, and the best-fitting model was chosen using CLIC. We find that the spatial extremal dependence is nonstationary with time, as the test statistic to validate the trend in the mixing proportion is statistically significant. This led to a negative trend in the range of extremal dependence, where its value in 2023 is approximately equal to half its value in 1970. This result is coherent with recent studies (Nicolet et al., 2016; Blanchet et al., 2018; Nicolet et al., 2018) showing that the strength of spatial dependence decreases in recent years for extreme events.
Although the complexity of the proposed model, it is flexible. As one can find the best space-time model to represent the studied data by changing the mixing max-stable models, the time-varying function of the mixing proportion (linear or nonlinear), or both.
As known, it is difficult to determine if a dependence structure of some data is asymptotically dependent or asymptotically independent (Wadsworth and Tawn, 2012), in future work, we plan to use the same framework of the proposed model in this paper for addressing this problem. We will mix a max-stable model with an inverted max-stable model using a time-varying mixing proportion. Such a model may be more flexible and appropriate for modeling the environmental data under the status of climate change.

Acknowledgements

The authors would like to thank Météo-France for supplying us with the data used in this work. Also, we acknowledge partial support from the PAUSE program, operated by the Collège de France.

References

Abu-Awwad, A.F., Maume-Deschamps, V., Pierre, R., 2020. Censored pairwise likelihood-based tests for mixing coefficient of spatial max-mixture models. Revista de Investigacion Operacional 41, 1–26.

Abu-Awwad, A.F., Maume-Deschamps, V., Pierre, R., 2021. Semiparametric estimation for space-time max-stable processes: an f-madogram-based approach. Statistical Inference for Stochastic Processes 24, 241–276.

Ahmed, M., Maume-Deschamps, V., Ribereau, P., Vial, C., 2017. A semiparametric estimation for max-mixture spatial processes. arXiv preprint arXiv:1710.08120 .

Bacro, J.N., Gaetan, C., Toulemonde, G., 2016. A flexible dependence model for spatial extremes. Journal of Statistical Planning and Inference 172, 36–52. https://doi.org/10.1016/j.jspi.2015.12.002.

Blanchet, J., Aly, C., Vischel, T., Panthou, G., Sané, Y., Diop Kane, M., 2018. Trend in the co-occurrence of extreme daily rainfall in west africa since 1950. Journal of Geophysical Research: Atmospheres 123, 1536–1551. https://doi.org/10.1002/2017JD027219.

Blanchet, J., Davison, A.C., 2011. Spatial modeling of extreme snow depth. The Annals of Applied Statistics 5, 1699–1725.

Buhl, S., Klüppelberg, C., 2016. Anisotropic brown-resnick space-time processes: estimation and model assessment. Extremes 19, 627–660. https://doi.org/10.1007/s10687-016-0257-1.

Castruccio, S., Huser, R., Genton, M.G., 2016. High-order composite likelihood inference for max-stable distributions and processes. Journal of Computational and Graphical Statistics 25, 1212–1229.

Cooley, D., Naveau, P., Poncet, P., 2006. Variograms for spatial max-stable random fields, in: Dependence in Probability and Statistics. Springer, New York, NY, pp. 373–390. https://doi.org/10.1007/0-387-36062-X_17.

Davis, R.A., Klüppelberg, C., Steinkohl, C., 2013. Max-stable processes for modeling extremes observed in space and time. Journal of the Korean Statistical Society 42, 399–414. https://doi.org/10.1016/j.jkss.2013.01.002.

Davison, A.C., Gholamrezaee, M.M., 2012. Geostatistics of extremes. Proceedings of the Royal Society A: Mathematical, Physical and Engineering Sciences 468, 581–608. https://doi.org/10.1098/rspa.2011.0412.

De Haan, L., 1984. A spectral representation for max-stable processes. The annals of probability 12, 1194–1204.

De Haan, L., Ferreira, A., 2006. Extreme value theory: an introduction. Springer, New York, NY. https://doi.org/10.1007/0-387-34471-3.

De Haan, L., Pereira, T.T., 2006. Spatial extremes: Models for the stationary case. The annals of statistics 34, 146–168. https://doi.org/10.1214/009053605000000886.

Embrechts, P., Koch, E., Robert, C., 2016. Space–time max-stable models with spectral separability. Advances in Applied Probability 48, 77–97. https://doi.org/10.1017/apr.2016.43.

Fawcett, L., Walshaw, D., 2014. Estimating the probability of simultaneous rainfall extremes within a region: a spatial approach. Journal of Applied Statistics 41, 959–976. https://doi.org/10.1080/02664763.2013.856872.

Gaume, J., Eckert, N., Chambon, G., Naaim, M., Bel, L., 2013. Mapping extreme snowfalls in the french alps using max-stable processes. Water Resources Research 49, 1079–1098. https://doi.org/10.1002/wrcr.20083.

Huser, R., Davison, A.C., 2014. Space–time modelling of extreme events. Journal of the Royal Statistical Society Series B: Statistical Methodology 76, 439–461.

Huser, R., Dombry, C., Ribatet, M., Genton, M.G., 2019. Full likelihood inference for max-stable data. Stat 8, e218. https://doi.org/10.1002/sta4.218.

Huser, R., Genton, M.G., 2016. Non-stationary dependence structures for spatial extremes. Journal of agricultural, biological, and environmental statistics 21, 470–491. https://doi.org/10.1007/s13253-016-0247-4.

Kabluchko, Z., Schlather, M., De Haan, L., 2009. Stationary max-stable fields associated to negative definite functions. The Annals of Probability 37, 2042–2065. https://doi.org/10.1214/09-AOP455.

Lindsay, B.G., 1988. Composite likelihood methods. Comtemporary Mathematics 80, 221–239.

Naveau, P., Guillou, A., Cooley, D., Diebolt, J., 2009. Modelling pairwise dependence of maxima in space. Biometrika 96, 1–17.

Nicolet, G., Eckert, N., Morin, S., Blanchet, J., 2016. Decreasing spatial dependence in extreme snowfall in the french alps since 1958 under climate change. Journal of Geophysical Research: Atmospheres 121, 8297–8310. https://doi.org/10.1002/2016JD025427.

Nicolet, G., Eckert, N., Morin, S., Blanchet, J., 2018. Assessing climate change impact on the spatial dependence of extreme snow depth maxima in the french alps. Water Resources Research 54, 7820–7840. https://doi.org/10.1029/2018WR022763.

Oesting, M., Naveau, P., 2020. Spatial modeling of heavy precipitation by coupling weather station recordings and ensemble forecasts with max-stable processes. arXiv preprint arXiv:2003.05854 .

Opitz, T., 2013. Extremal t processes: Elliptical domain of attraction and a spectral representation. Journal of Multivariate Analysis 122, 409–413. https://doi.org/10.1016/j.jmva.2013.08.008.

Padoan, S.A., Ribatet, M., Sisson, S.A., 2010. Likelihood-based inference for max-stable processes. Journal of the American Statistical Association 105, 263–277.

Ribatet, M., 2013. Spatial extremes: Max-stable processes at work. Journal de la Société Française de Statistique 154, 156–177.

Ribatet, M., 2017. Modelling spatial extremes using max-stable processes, in: Nonlinear and Stochastic Climate Dynamics. Cambridge University Press, Cambridge, p. 369–391. https://doi.org/10.1017/9781316339251.014.

Ribatet, M., 2022. Spatialextremes: Modelling spatial extremes. r package version 2.1-0. https://CRAN.R-project.org/package=SpatialExtremes.

Ribatet, M., Dombry, C., Oesting, M., 2016. Spatial extremes and max-stable processes, in: Extreme value modeling and risk analysis: methods and applications. Chapman and Hall/CRC, New York, pp. 179–194. https://doi.org/10.1201/b19721.

Saunders, K., Stephenson, A.G., Taylor, P.G., Karoly, D., 2017. The spatial distribution of rainfall extremes and the influence of el niño southern oscillation. Weather and climate extremes 18, 17–28. https://doi.org/10.1016/j.wace.2017.10.001.

Schlather, M., 2002. Models for stationary max-stable random fields. Extremes 5, 33–44. https://doi.org/10.1023/A:1020977924878.

Schlather, M., Tawn, J.A., 2003. A dependence measure for multivariate and spatial extreme values: Properties and inference. Biometrika 90, 139–156.

Smith, R.L., 1990. Max-stable processes and spatial extremes. Unpublished manuscript .

Varin, C., Reid, N., Firth, D., 2011. An overview of composite likelihood methods. Statistica Sinica 21, 5–42.

Varin, C., Vidoni, P., 2005. A note on composite likelihood inference and model selection. Biometrika 92, 519–528.

Wadsworth, J.L., Tawn, J.A., 2012. Dependence modelling for spatial extremes. Biometrika 99, 253–272.